HYBRID POMERON MODEL OF EXCLUSIVE CENTRAL DIFFRACTIVE PRODUCTION

Robi Peschanski

IPhT, Institut de Physique Théorique, CEA/Saclay
91191 Gif-sur-Yvette cedex, France[†]
robi.peschanski@cea.fr

M. Rangel

LAFEX, Centro Brasileiro de Pesquisas Fisícas, Rio de Janeiro, Brazil
rangel@cbpf.br

C. Royon

CEA/IRFU/Service de Physique des Particules, CEA/Saclay
91191 Gif-sur-Yvette cedex, France
royon@hep.saclay.cea.fr

(Received April 3, 2009)

Central diffractive production of heavy states (massive dijets, Higgs boson) is studied in the exclusive mode using a new *Hybrid Pomeron Model*. Built from Hybrid Pomerons defined by the combination of one hard and one soft color exchanges, the model describes well the centrally produced diffractive dijet data at the Tevatron. Predictions for the Higgs boson and dijet exclusive production at the LHC are presented.

PACS numbers: 12.38.–t, 13.60.Hb

1. Introduction: The hybrid Pomeron

Central diffractive production of heavy objects in its *exclusive* mode (no other particle produced in the central rapidity region) appears as a promising complementary tool for the study of new particles at the LHC, such as the Higgs boson. Indeed, for instance, the mass determination can be made quite precise if both incident protons are detected and measured in forward detectors located at 220 and 420 m from the interaction point at the LHC [1, 2]. One expects to take advantage of the absence of other particles than

[†] URA 2306, unité de recherche associée au CNRS.

the decay products in the central rapidity region and some other interesting aspects such as the depletion of b-quark production due to the helicity rule specific of this production mode [3]. The key problem of central diffractive production in the exclusive mode is to determine its rate as a function of *e.g.* the Higgs boson mass or the minimum p_{T} of the jets. Experimental results on massive dijet production at the Tevatron have shown indirect evidence for exclusive production, by comparison with models of *inclusive* diffractive production. Inclusive models [4,5] agree to point out an excess of events over the inclusive spectrum in the kinematical region where exclusive production is expected to contribute.

The experimental interest of central exclusive production, in the first place for the Higgs boson and γ induced processes, and the preparation of concrete proposals at the LHC are a major incentive for theorists to work out reliable predictions for the production cross-section, which could serve as a basis for the necessary data simulations. This task is not easy since central diffractive processes imply both hard subprocesses, related to the high mass of the centrally produced states, and soft ones which are typical of diffractive events which leave intact the initial particles *e.g.* protons at the LHC. In some sense one could say that central diffractive production is expected to combine the "hardest" events such as the production of massive Higgs bosons or of any high mass object (dijet, diphoton ...), with the "softest" ones, since the initial particles remain totally intact (up to a loss of energy not bigger than 10%). This reveals the potentially *hybrid* character of central diffractive production.

On the theoretical ground, different mechanisms of exclusive central diffraction have been proposed since years [6], but we will restrict to two classes of models which are based on the exchange of colorless objects, in order to take into account the diffractive property. Indeed, any colored object would generate particle production in the whole rapidity interval[1]. One class is based on the exchange of two Pomerons, where the Pomeron is the colorless exchange which appear in *e.g.* elastic reactions; it can be called the Non Perturbative Model (NPM) and was based on a typical soft interaction hypothesis, which comes from the Bialas–Landshoff mechanism [8] originally proposed for central diffractive production. It has an *inclusive* version which describes the inclusive diffractive dijet production [9], while its *exclusive* version has been studied in Ref. [10]. One another class of models is based on the exchange of two gluons at each vertex for the exclu-

[1] One notable exception is the Soft Color Interaction (SCI) model [7] where a colorful exchange is compensated by a phenomenological soft color interaction at long distance, which generates a gap in rapidity. We do not consider this model in the further discussion since it would need modifications to describe the CDF measurement of the dijet mass fraction [5].

sive production [11] called KMR (from the author names) in the following. For both models there exists a detailed phenomenological discussion (see *e.g.* [5]) based on dedicated simulations.

Let us recall the present status of this physically meaning discussion. The inclusive production mechanism based on the NPM [9] gives satisfactory results when compared to Tevatron data. Using this agreement, the extraction of the exclusive component in the DPE framework becomes possible, since it appears to be necessary to include it in a well-defined region of phase-space. When comparing [4, 5] the extracted dijet cross-section and spectra with the models, it appears that the KMR model [11] gives a better description of the results than NPM [9]. The main reason is that it takes into account the Sudakov suppression factors preventing the cross-sections to include the gluon radiation normally associated with the production of a massive object. The soft Pomeron exchanges of NPM [9] do not contain these perturbative QCD factors and give a too flat distribution as a function of the minimum transverse momentum $p_{\mathrm{T}}^{\mathrm{min}}$ of the jet [5]. As a consequence, the prediction for the Higgs boson cross-section, which was similar for both models for a light Higgs boson [12], has a different form as a function of the Higgs boson mass, being steeper for the KMR model [11] than for NPM [9]. It is expected that the NPM model in Ref. [9] works at low masses (for instance for χ_c production [13]) whereas a model including a hard contribution may be valid at higher masses.

Our motivation is to keep the Double Pomeron Exchange (DPE) hypothesis, while taking into account the fact that the diffractive production process is expected to be a mixture of soft and hard color exchanges. Indeed, the notion of a hard Pomeron (associated in QCD with the summation of ladder diagrams in the leading or next-to-leading logarithmic approximation (LLA) of the perturbative expansion) is a theoretical result of QCD [14]. Moreover it has been successfully compared with data in (hard) inclusive diffraction (see, *e.g.* [15, 16]) and exclusive vector meson production [18]. The example of heavy vector meson production, in particular, is well suited for our approach since it corresponds to the (quasi-) elastic production of a heavy state, which can be formulated in the framework of a hard Pomeron exchange.

In the theoretical calculations, the hard Pomeron appears to correspond to ladder diagrams connecting two exchanged reggeized colored gluons [14]. However, in central diffractive production, one could expect to have two different colored exchanges, one hard and one soft. It would correspond physically to two time scales, one short corresponding to the heavy state production, and one long corresponding to the necessary color neutralization. Hence, the qualitative picture of central diffractive production which we formulate is a DPE process in which each Pomeron exchange at the ver-

tex would correspond to *hybrid* Pomerons with two different types of color exchanges one soft and one hard. It would correspond to an $effective$ way of summing ladder diagrams between hard and soft colored reggeized gluons, which precise calculation remains beyond our scope (and beyond the present knowledge of non perturbative QCD physics).

The plan of the paper is the following. In the next section, we shall formulate the Hybrid Pomeron Model (HPM) and determine its parameters obtained from known soft and hard Pomeron processes. In Section 3, we will show its good description of exclusive dijet production extracted from data at the Tevatron and the prediction for Higgs Boson and dijet production at the LHC. The last section is for discussions, conclusions and an outlook.

2. Formulation: The Hybrid Pomeron Model

The model, adopting as a starting point the idea of the original Bialas–Landshoff formulation, consists in defining effective propagators and couplings for the colored exchanges associated with central DPE processes, see Fig. 1. However, by contrast with the original NPM model of Ref. [8], we introduce two types of propagators and couplings, depending of its soft or hard character. The soft propagator $D_{\rm S}$ and coupling $G_{\rm S}$ are exactly those which appear in the original description of the Bialas–Landshoff model [8], themselves connected to the soft Pomeron Landshoff–Nachtmann formulation [17] of the elastic cross-section, see Fig. 2. They are constrained to describe the elastic hadronic cross-section, which fixes its parameters.

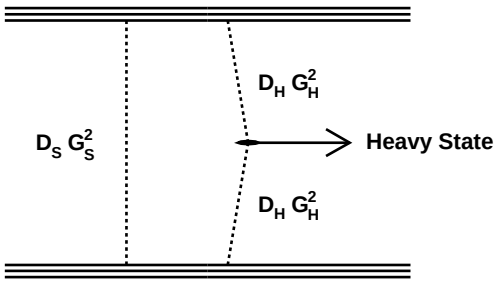


Fig. 1. Hybrid Pomeron Model. The dotted lines schematically represent the colored exchanges. They are formulated in terms of effective propagators for soft and hard exchanges (resp. $D_{\rm S}$ and $D_{\rm H}$) and couplings (resp. $G_{\rm S}$ and $G_{\rm H}$), see text.

The new aspect, w.r.t. the original formulation [8], is to introduce similarly effective propagators and couplings $D_{\rm H}$ and coupling $G_{\rm H}$ for hard Pomeron processes. Since we are formulating a *Hybrid Pomeron Model* (HPM), we would optimally need the resummation of QCD ladder diagrams corresponding to both soft and hard colored exchanges. As we see in Fig. 1,

the hard exchange produces the heavy state object ($D_{\mathrm{H}}G_{\mathrm{H}}^2$) while the colorless aspect of the exchange is ensured via the emission of a soft additional gluon ($D_{\mathrm{S}}G_{\mathrm{S}}^2$). This means that most of the available momentum is carried away by one of the gluons, the hard one, while the soft one carries only a very small fraction of the proton momentum. The hard part of the HPM model will be based on hard physics measured at HERA (for instance the proton structure function F_2) while the soft part will be based on usual soft cross-section measurements. In the case of simple elementary gluon exchanges, as developed in the model [11], the problem is perturbatively tractable[2], since the loop kinematics enforces a (semi-) perturbative calculation. However, when considering Pomeron ladders, the gluon loop constraint, characteristic for the mechanism of [11], does not hold and thus one relies on the Bialas–Landshoff modified picture in order to include both soft and hard effective color exchanges, see Fig. 1. Hence our proposal is to start with the description of hard Pomeron scattering in terms of effective hard colored propagators D_{H} and couplings G_{H}, in the same way as for the soft color exchanges in [8].

For this sake we consider the well-known dipole–proton amplitudes which appears in the QCD description of many hard processes. They will be used to determine the effective propagators and couplings. In that sense, it is possible to fix the parameters of the model using hard physics measurements at HERA, especially from the measurements of the proton structure function and the vector meson production cross-sections. In this basic process, a dipole of size r experiences an elastic scattering with the proton. Since the dipole–proton amplitude, corresponding to a hard Pomeron exchange, appears in the formulation of different observables, its parameters are well determined, and this gives the possibility to define the appropriate hard propagators D_{H} and couplings G_{H}, in the same way as was done for the soft ones, but with the advantage that we have a theoretical control on its precise QCD formulation.

A comment has to be made at this stage. The main new aspect of HPM is to introduce a formulation for hard color exchanges. Since it is a phenomenological effective description of diagrams going beyond elementary gluon exchanges, it aims at keeping the physical image of two different time scales and thus of two different types of effective propagators. Hence the virtuality associated with the hard color exchanges cannot be transferred to the other color exchange through the loop kinematics, as is the case in the model [11]. On the other hand the inclusion of hard color exchanges in the DPE formulation is expected to (and indeed will, as we shall see) correct the drawbacks of the initial soft model.

[2] At least partly, since the considered models have to correct for the rapidity gap survival probability, corresponding to the interaction between incident particles [19, 20].

2.1. Soft color exchange

We evaluate the non-perturbative gluon propagator from the elastic proton–proton data, see Fig. 2. Following Landshoff–Nachtmann proposal [17], the elastic hadron–hadron scattering is represented by the contributions of elastic valence quark scattering mediated by a non-perturbative model for gluon exchange. The elastic quark–quark amplitude in terms of soft propagator and coupling writes

$$A_{qq} \equiv G_{\rm S}^2 \; D_{\rm S} = s^{\alpha_{\mathcal{P}}(t)-1} \; G_{\rm S}^2 \; D_{\rm S}^{(0)} \; e^{t/\mu_{\rm S}^2} \, , \tag{1}$$

where s is the total c.o.m. energy, t the transfer quadrimoment squared whose dependence is approximated by an exponential slope given by $\mu_{\rm S}$ and

$$\alpha_{\mathcal{P}}(t) \equiv \alpha_{\mathcal{P}}(0) + \alpha'_{\mathcal{P}} t = 1 + \epsilon + \alpha'_{\mathcal{P}} t \tag{2}$$

is the soft Pomeron Regge trajectory [21], with $\epsilon \sim .08$ being the Pomeron "anomalous intercept". Note that we have incorporated the factors due to reggeization [8] in the definition of the propagators. This is required in order to take into account the different Regge parameters (and in particular the known different energy dependence) between the soft and hard Pomeron ingredients. In other terms the *hybrid Pomeron* will have an intermediate energy dependence compared to the soft and the hard Pomeron's ones.

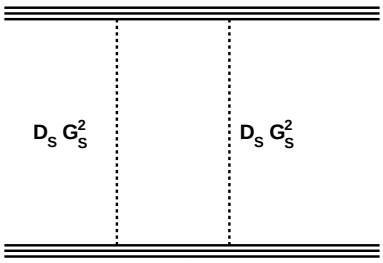


Fig. 2. Proton–proton elastic scattering in the Landshoff–Nachtmann formulation. The elastic amplitude is described by two-color exchanges associated with "non-perturbative" gluon propagators $D_{\rm S}$ and couplings $G_{\rm S}$ [8].

All in all, the differential elastic hadronic cross-section, from which the relevant parameters will be obtained, is given in a suitable normalization, by

$$\frac{d\sigma}{dt} \equiv \{9A_{qq}\}^2 = \frac{|3\beta|^4}{4\pi} s^{2\alpha_{\mathcal{P}}(0)-2} \exp\left[(4b + 2\alpha'_{\mathcal{P}} \log s) \; t\right] \, , \tag{3}$$

where the parameter β can be obtained [8] from the total cross-section and b from the elastic form factor or equivalently, from the differential cross-section. Note that the factor $\{9A_{qq}\}$ comes from the number of valence quark combinations, which are considered independent in the Landshoff–Nachtmann formulation.

Using the effective propagator and coupling formulation of (1), one finally determines

$$\begin{aligned} \mu_{\rm S}^{-2} &= 2b + \alpha' \log s \,, \\ \left[G_{\rm S}^2 \; D_{\rm S}\right]^2 &= \sqrt{4\pi}\beta^2 e^{t/\mu_{\rm S}^2} \,. \end{aligned} \tag{4}$$

It is relevant to note the exponential transverse momentum cut-off $\mu_{\rm S}$, which will limit the loop integration of the HPM model, see Fig. 1. This is a characteristic feature of the HPM which distinguishes it from the perturbative mechanism of [11], see further the theoretical discussion.

2.2. Hard color exchange

For the definition of the propagator and coupling of the hard color exchange, we will use the well-known hard Pomeron for the dipole proton elastic amplitude calculated from perturbative QCD using as a starting point the Balitsky–Fadin–Kuraev–Lipatov (BFKL) equation [14]. It is convenient to open the possibility of saturation effects, even if they are not expected to be important in the kinematical domain we are interested in. Indeed, this form of the dipole proton amplitude (eventually modified by saturation contributions) has been proven to be phenomenologically successful in the description of proton total and diffractive structure functions [15] and, more importantly for our analysis, for structure function F_2 measured at HERA including the charm contribution [22] for vector meson elastic differential cross-section [18] and for inelastic diffraction [16], which will be used for parameter fixing. Hence the model we will adopt for dipole–proton elastic scattering contains saturation effects and |t| dependence [18].

We start with the following amplitude in terms of the BFKL kernel. One writes

$$\mathcal{N}(r,Y) = \int\limits_{\mathcal{C}} \frac{d\gamma}{2i\pi}\, \mathcal{N}_0(\gamma)\, r^{2\gamma} \exp\left\{\bar{\alpha}\chi(\gamma)Y\right\} \,, \tag{5}$$

where $\chi(\gamma)$ is the Mellin transform of the BFKL kernel [14]. $\mathcal{N}_0(\gamma)$ contains information on the coupling to the proton and other normalization contributions.

The effect of saturation, through nonlinear damping factors, is known [23] to select a *critical* value $\gamma_{\rm c}$. This corresponds to a "anomalous dimension" $d_{\rm c} = \gamma_{\rm c} - 1$ which is characteristic of a (saturation-corrected) hard Pomeron. In a more concrete way, the authors of [18] make use of a model for the dipole–proton amplitude [24] which successfully describes the precise proton structure function data.

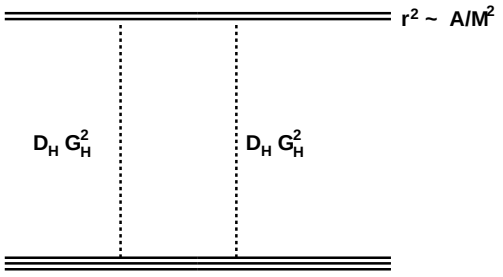


Fig. 3. Dipole–proton elastic amplitude. The elastic amplitude is described by two-color exchanges associated with hard colored propagators $D_{\rm H}$ and couplings $G_{\rm H}$, see text. As well-known, the dipole size is approximately related to the vector meson mass $r^2 \propto M^{-2}$.

$$\begin{aligned} \mathcal{N}(r,Y) &= N_0\ (P_{\rm H})^{\gamma_{\rm c}} \exp\left(-\frac{\log^2 P_{\rm H}}{2\kappa\lambda Y}\right) \exp(Bt)\,, \\ P_{\rm H} &= (r/r_{\rm S})^2\,, \\ \\ r_{\rm S}^2 &= r_0^2 \exp(-\lambda Y)\,, \end{aligned} \tag{6}$$

where $Q_{\rm S} \equiv 2/r_{\rm S}$ is the well-known saturation scale, the term $\exp(-B|t|)$ has been added in order to take into account the momentum transfer dependence in vector meson production [18]. The exponential term in (6) takes into account the contribution from the kernel variation around the saddle-point. Note that this amplitude works [24] in the region $P_{\rm H} < 1$, which is safely true in our case. The saturation corrections are expected to be negligible in that region.

It is important to notice at this stage that we need to consider *amputated* amplitudes, that is multiplying the expressions (5,6) of the dipole–proton amplitude by a factor r^{-2}. Indeed, we have to remove from the usual dipole proton amplitude the factor corresponding to the geometrical dimension of the dipole cross-section proportional to r^2, or in other words the gluon dipole coupling. This factor has to be removed in order to define properly the couplings and propagators of the hard effective color exchanges, which would be valid for any massive state. We are interested in applying our formalism to the exclusive production of massive dijets or the Higgs boson and thus have to switch from a dipole state to the wave function corresponding to the heavy state under study.

In the kinematical configuration of central diffractive production, we have at each hard color exchange vertex (see Fig. 1)

$$Y = -\log\xi\,, \qquad \text{and} \qquad r^2 \sim \frac{A}{M^2}\,, \tag{7}$$

where we used a very simple[3] relation (with $A \sim 7$ phenomenologically) between the mass M of the heavy state and the corresponding dipole size r to be considered. The normalization factors N_0 for the amplitude and the scale r_0 are also determined phenomenologically from HERA data. For dipole–proton scattering, we assume also a dominance of "valence" quark–quark scattering and 6 quark–quark combinations are allowed.

The main characteristic feature of the hard Pomeron by contrast with the soft one is that it has a non trivial dependence on Y and r (translating into a non trivial ξ and M dependence in the central diffraction kinematics) through the anomalous dimension $\gamma_{\rm c}$. Indeed, this perturbative QCD feature gives a dependence on the hard scale which has to be contrasted with the one coming from the Sudakov form factors, see further the theoretical discussion in section IID. It acquires also a different, faster, energy dependence through the dependence on $P_{\rm H}$ in (6).

Using concretely the parameters from the fit to the HERA data [18, 22], one finds the following expression for the couplings and propagators of the hard gluon exchanges:

$$\begin{aligned} \mu_{\rm H}^2 &= B^{-1} \sim 0.25\,, \\ \left[G_{\rm H}^2 D_{\rm H}^{(0)}\right]^2 &= N_0 \times r^{-2} \times P_{\rm H}^{\gamma_{\rm c}} \exp\left(\frac{\log^2 P_{\rm H}}{2\kappa\lambda \log\xi}\right)\,, \end{aligned} \tag{8}$$

where we have used the values for κ, λ, B (see formulae (6)) taken from the phenomenological analysis [18, 22] of massive vector mesons, charm and structure function measurements at HERA [26]. The different parameters used in the model are given in Table I.

2.3. The central diffractive cross-section

All in all, and following the scheme depicted in Fig. 1, one has the following matrix element for the central exclusive diffractive production of a massive state:

$$|M|^2 = \left(D_{\rm S} G_{\rm S}^2\right)^2 \left(\left[D_{\rm H} G_{\rm H}^2\right]_1\right)^2 \left(\left[D_{\rm H} G_{\rm H}^2\right]_2\right)^2 |M_{\hat{\sigma}}|^2\,. \tag{9}$$

The notation $[D_{\rm H} G_{\rm H}^2]_i$, $i = 1, 2$ is used to distinguish the hard colored exchanges from each vertex, see Fig. 1. $M_{\hat{\sigma}}$ is the hard process matrix element for the considered produced massive state.

[3] More refined wave function analyses are straightforward extensions of our formalism.

TABLE I

List of parameters used in the HPM. The second column give the default values used in the model, the third one the range of values used for systematics coming from the fit uncertainties to F_2 data, and the fourth one the values of parameters when heavy quarks are also considered in the model (see text).

Parameter	Central value	Uncertainties	Charm included
Hard parameters			
N_0	0.7	—	0.7
Q_0	0.254 GeV	0.243–0.263	0.298
R_p	3.277 GeV^{-1}	3.233–3.321	3.344
$\gamma_{\rm C}$	0.6194	0.6103–0.6285	0.7376
κ	9.9	—	9.9
λ	0.2545	0.2494–0.2596	0.2197
B	2	—	2
$\mu_{\rm H}$	0.5	—	0.5
Soft parameters			
$\alpha_P(0)$	1.08	—	1.08
α'	0.06	—	0.06
β	4	—	4
b	4	3–5	4

In parallel with the approach of Ref. [8], the cross-section is written as:

$$\begin{aligned}\sigma \;=\; & 81\frac{2s}{(2\pi)^5}\left[G_{\rm S}^2\; D_{\rm S}^{(0)}\right]^2 \\ & \times \int d^4p_1 d^4p_2\; \delta\left(p_1^2\right)\delta\left(p_2^2\right)\delta\left((p_a+p_b-p_1-p_2)^2-M^2\right) \\ & \times \left(\frac{s}{s_1}\right)^{2\alpha_{\mathcal P}(t1)-2}\left(\frac{s}{s_2}\right)^{2\alpha_{\mathcal P}(t2)-2} \\ & \times e^{2bt_1}e^{2bt2}\left[G_{\rm H}^2\; D_{\rm H}^{(0)}\right]_1^2\left[G_{\rm H}^2\; D_{\rm H}^{(0)}\right]_2^2|M_{\hat\sigma}|^2\,. \end{aligned} \tag{10}$$

Using relation [27]

$$\int d^4p_i\delta(p_i^2) = -\frac{1}{2}\int d\xi_i\; d^2\vec{v_i}\,; \qquad \frac{s}{s_i}=\frac{1}{\xi_i}\,, \tag{11}$$

where $\vec{v_i}$ is the transverse momentum of the final protons and changing the variable v_i to $|t_i|$ using $|\vec{v_i}|^2=(1-\xi_1)|t_i|$, one finally finds:

$$\begin{aligned}\sigma \;=\; & \frac{81}{2(2\pi)^3}\left[G_{\rm S}^2\; D_{\rm S}^{(0)}\right]^2\prod_{i=1,2}\int\!\!\int d\xi_i d|t_i|\;\frac{1-\xi_i}{{\xi_i}^{2\epsilon}}\exp\left\{2(b-\alpha'_{\mathcal P}\log\xi_i)t_i\right\} \\ & \times\left[G_{\rm H}^2\; D_{\rm H}^{(0)}\right]_i^2\times|M_{\hat\sigma}|^2\,. \end{aligned} \tag{12}$$

2.4. Theoretical issues: offshellness and Sudakov form factors

Let us describe the hybrid model mechanism for central diffractive production, see Fig. 4(a), by comparison with the non-perturbative one (*cf*. Bialas–Landshoff), see Fig. 4(b), and the perturbative (KMR) mechanism, see Fig. 4(b).

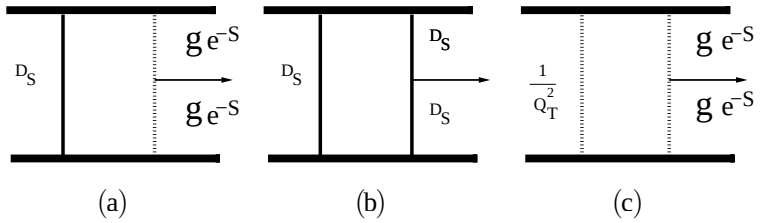


Fig. 4. Comparison of central diffractive production mechanisms. The continuous lines, (resp. hatched lines) correspond to the non-perturbative (resp. perturbative) propagators. g represent the gluon distributions (see text). $\exp -S/2$ correspond to the contributions of the Sudakov form factor. (a) The hybrid model mechanism; The non-perturbative (Bialas–Landshoff) mechanism; (c) The perturbative (KMR) mechanism. In the hybrid model (Fig. 4(a)) the non-perturbative propagator $D_{\rm S}$ replaces the perturbative propagator $1/Q_{\rm T}^2$ of the left exchanged gluon (Fig. 4(c)).

In the case of the hybrid model mechanism, one perturbative gluon propagator (the one corresponding to the left gluon exchange in Fig. 4(c)) is replaced by the non-perturbative one $D_{\rm S}$ with a Gaussian dependence in transverse momentum $Q_{\rm T}^2$, see formula (4). This provides a cut-off on large values of the transverse momentum which thus dominates over the ultraviolet cut-off due to the Sudakov form-factor in the case of the perturbative mechanism.

Let us examine more quantitatively this mechanism and the modification of the role of Sudakov form factors w.r.t. the perturbative mechanism schematized in Fig. 4(b). For this sake we consider an expression for the loop-integration general enough to embody the three typical cases: non-perturbative, perturbative and hybrid. Such an expression enters (as a square) in the cross-section expression. for simplicity, we choose scalar Higgs boson production for this discussion, but its validity extends to the other cases. On a general footing, one may write the typical loop integration as

$$I = \int \mathcal{P}(Q_{\rm T}^2)\, dQ_{\rm T}^2 \; f(\xi_1, M_H^2; Q_{\rm T}^2; \dots)\; f(\xi_2, M_H^2; Q_{\rm T}^2, \dots)\;, \qquad (13)$$

where $\mathcal{P}(Q_{\rm T}^2)\, dQ_{\rm T}^2$ is the integration measure corresponding to the gluon propagators to which one adds the loop contribution from the Higgs vertex, and $f(\xi_i, M_H^2; Q_{\rm T}^2; \cdots)$ are the general probability distributions of the gluons

in the incident protons producing by gluon–gluon fusion the Higgs boson of mass M_H. The dots are for the variables nonrelevant for the loop integration. Note that these distributions may depend on *both* scales M_H^2 and $Q_{\rm T}^2$. Let us consider successively the three types of models.

(i) For the hybrid model, see Fig. 4(a), one has

$$\begin{aligned} \mathcal{P}(Q_{\rm T}^2)\, dQ_{\rm T}^2 \;&\sim\; \frac{dQ_{\rm T}^2}{Q_{\rm T}^2}\, D_{\rm S}(-Q_{\rm T}^2)\,, \\ f(\xi_i, M_H^2; Q_{\rm T}^2; \dots) \;&\sim\; e^{-S(Q_{\rm T}^2, M_H^2)/2}\; g(\xi_i, M_H^2; Q_{\rm T}^2; \dots)\,, \end{aligned} \tag{14}$$

where $D_{\rm S} \propto e^{-t/\mu_{\rm S}^2} = e^{-Q_{\rm T}^2/\mu_{\rm S}^2}$, have a Gaussian behaviour in transverse space, with an ultra-violet cut-off $\mu_{\rm S}$ and e^{-S} is the overall Sudakov form factor (to be discussed below).

(ii) For the non-perturbative model, see Fig. 4(b), one writes

$$\begin{aligned} \mathcal{P}(Q_{\rm T}^2)\, dQ_{\rm T}^2 \;&\sim\; Q_{\rm T}^2 dQ_{\rm T}^2\; D_{\rm S}(-Q_{\rm T}^2)\,, \\ f(\xi_i, M_H^2; Q_{\rm T}^2; \dots) \;&\sim\; D_{\rm S}(-\xi_i Q_{\rm T}^2)\,, \end{aligned} \tag{15}$$

where all functions have a Gaussian behaviour in transverse space, namely $D_{\rm S} \propto e^{-t/\mu_{\rm S}^2} = e^{-Q_{\rm T}^2/\mu_{\rm S}^2}$, see (4).

(iii) For the perturbative approach, see Fig. 4(c), the expression is[4]:

$$\begin{aligned} \mathcal{P}(Q_{\rm T}^2)\, dQ_{\rm T}^2 \;&\sim\; \frac{dQ_{\rm T}^2}{Q_{\rm T}^4}\,, \\ f(\xi_i, M_H^2; Q_{\rm T}^2; \dots) \;&\sim\; e^{-S(Q_{\rm T}^2, M_H^2)/2} \frac{\partial}{\partial \ln Q_{\rm T}^2} G(\xi_i, Q_{\rm T}^2)\;, \end{aligned} \tag{16}$$

where $G(\xi_i, Q_{\rm T}^2)$ are the gluon distributions in the initial protons and e^{-S} is the Sudakov form factor[5].

The comparison of the expressions (14) with (15) and (16) calls for the following comments.

Sudakov form factors.

Concerning the Sudakov form factors, the full expression including single logs has an important phenomenological impact (*e.g.* [25]), but for the purpose of our theoretical discussion, we may focus on the double-log approximation for the case of $Q_{\rm T}^2 \ll M_H^2$, namely

[4] A recent clear reviewing can be found in [25].

[5] To be complete, the expression used in the KMR model contains also terms of the kind $\frac{\partial e^{S/2}}{\partial \ln Q_{\rm T}^2} \times G(\xi_i, Q_{\rm T}^2)$, with no important relevance for our discussion.

$$S\left(Q_{\rm T}^2, M_H^2\right) \sim \frac{N_c \alpha_{\rm S}}{4\pi} \ln^2\left(\frac{Q_{\rm T}^2}{M_H^2}\right), \tag{17}$$

a priori, Eq.(17) leads to a lower bound on $Q_{\rm T}^2$, namely $e^{-\kappa} \lesssim \frac{Q_{\rm T}^2}{M_H^2}$, with $\kappa^2 = \frac{4\pi}{N_c \alpha_{\rm S}}$. In the perturbative case (Fig. 4(c)) the role of the Sudakov form factor is two-fold. In the infra-red, it regularizes the propagators' pole of $\mathcal{P}(Q_{\rm T}^2)$, while in the ultra-violet, it sets the scale related to the Higgs boson mass.

However, in the hybrid case (Fig. 4(a)) the Sudakov factor has a modified role. It is still required to remove the logarithmic divergence (instead of quadratic in the perturbative approach) of the integration measure, but it is not operative at large $Q_{\rm T}^2$, since there already exists an ultra-violet cut-off due to the non-perturbative scale $\mu_{\rm S}$. The integration is concentrated at rather small $Q_{\rm T\,min}^2 \sim M_H^2\ e^{-\kappa}$, and the maximal offshellness is thus much smaller than the hard scale related to the produced heavy state, namely $Q_{\rm T\,max}^2 \sim \mu_{\rm S}^2 \ll M_H^2$.

In the non-perturbative Bialas–Landshoff approach, (Fig. 4(b), the loop integration boils down to a simple Gaussian integration due to the Landshoff–Nachtmann model for the non-perturbative propagators. The offshellness of the propagators is thus limited by the non-perturbative cut-offs in transverse space.

Gluon distributions.

In the case of the hybrid mechanism and due to the restricted offshellness due to the non-perturbative propagator in (14), the unintegrated gluon distributions $g(\xi_i, M_H^2; Q_{\rm T\,min}^2)$ can be approximately factorized out. They depend on the hard scale M_H^2 but correspond to tranverse momenta $Q_{\rm T\,min}^2 \ll m_H^2$. Hence, the unintegrated gluon distributions $g(\xi_i, M_H^2; Q_{\rm T}^2; \dots)$ cannot be identified as the derivatives $\frac{\partial G(\xi_i, Q_{\rm T}^2)}{\partial \ln Q_{\rm T}^2}$ of the gluon structure functions. This is legitimate only when there is a strong ordering of the transverse momenta.

In order to look for an appropriate form of the gluon distributions, we note that the hard scale is given by the heavy state mass (being a dijet at large mass, a Higgs boson or else) and not by the transverse momentum. This is characteristic of elastic amplitudes involving a heavy state, such as the deep inelastic total cross-section or the elastic production of a heavy meson. In all those cases, one successfully uses the hard BFKL Pomeron, see *e.g.* Refs [15, 18]. Indeed, the hard Pomeron which has exactly these properties: it is dominated by a hard scale but the transverse momenta are not ordered and quite limited in some intermediate range (here of order

($Q^2_{\mathrm{T}\,\mathrm{min}}$). In our simple phenomenology-inspired hybrid model it is represented, up to constants, by the hard propagators discussed in Section 2.2, which are extracted from the description of hard exclusive diffractive processes such as the deep-inelastic total cross-sections or, equivalently from elastic vector meson production. Beyond our phenomenological model, a direct calculation of the relevant gluon distributions is beyond the scope of our study and thus deserves further work.

In summary, the Sudakov factors are still present and allow for a regularisation of the logarithmic divergence at small Q^2_{T} and they contribute to the (smallness of the) normalisation, but the hard scale is set through a different mechanism derived from the hard Pomeron properties.

Helicity rule. Concerning the matrix element describing the produced heavy state, it is known that the $J_z = 0$ rule applies as well in the perturbative framework (through the $J_z = 0$ matrix element) as in the non-perturbative case (using the color decomposition of the Pomeron exchange, see *e.g.* Ref. [27] for a detailed discussion). Note that in the second case, the $J_z = 0$ rule is satisfied in a process which is definitely at low Q_{T}, by contrast with the perturbative one. We thus expect the helicity rule to remain valid also in the hybrid model case, and thus apply it to our phenomenological model. We postpone more developed calculations to a further publication.

3. Comparison with dijet CDF data

3.1. Model implementation in FPMC

The model has been fully implemented in FPMC [28], using the parameters defined in the previous sections. The different parameters in the hard part of the model come mainly from a fit to HERA data (structure function F_2, charm and vector meson data) inspired by saturation models. By default, we take the parameters from a fit to the diffractive structure function F_2 measured by the H1 and ZEUS Collaborations at HERA [22]. The systematics uncertainties on the fit parameters define the systematic uncertainties of our model. In addition, it is possible to include heavy quarks in the model [22], and compare it to the vector meson production cross-section [18], which leads to different parameters of the model (see Table I). The difference of the results with and without including charm effects is also a kind of systematic uncertainty in the model and will be discussed further in the paper. In addition, the parameters related to the soft exchange come from the Donnachie–Landshoff model. All parameters are given for reference in Table I. The only parameter in the model is the free normalisation which we will obtain from a fit to the CDF exclusive diffractive measurements. Implicitly, the normalisation will thus include the survival probability. Note that the ratio of the survival probabilities between the Tevatron (0.1) and the LHC (0.03) is taken into account when we predict later on the cross-sections at the LHC.

The implementation in FPMC [28] allows to interface the hybrid model with a jet algorithm after hadronisation performed in HERWIG [29]. The standard jet algorithm [30] used by the CDF Collaboration has been implemented so that we are able to compare directly our model with the CDF measurements of exclusive events.

3.2. Comparison with CDF data

To test the accuracy of the model it is useful to compare it with the CDF measurements of exclusive events in the dijet channel at the Tevatron [4, 5]. CDF used the dijet mass fraction to quantify the amount of exclusive events. The dijet mass fraction, namely the ratio of the dijet mass to the total mass in dijet events, is expected to peak around 1 for exclusive events since two jets and nothing else are produced in the final state while inclusive events show lower values of the dijet mass fraction. The comparison between the CDF measurement and what is expected from inclusive diffraction based from quark and gluon densities measured at HERA (including the survival probability) leads to an estimate of the exclusive event cross-section. The result is given in Fig. 5. Data points show the exclusive cross-section for jets with a transverse momentum greater than a threshold value given in abscissa. To compare with the expectation from HPM, the FPMC Monte Carlo was interfaced with the jet cone algorithm used by the CDF Collaboration at hadron level. Since the normalisation is not determined by the model, we choose to fix it using the CDF measurement. The global normalisation is obtained by fitting our predictions to the CDF measurement given in Fig. 5. The normalisation is found to be: $3.85 \times 10^{-4} \pm 1.89 \times 10^{-4}$ with $\chi^2 = 0.67$

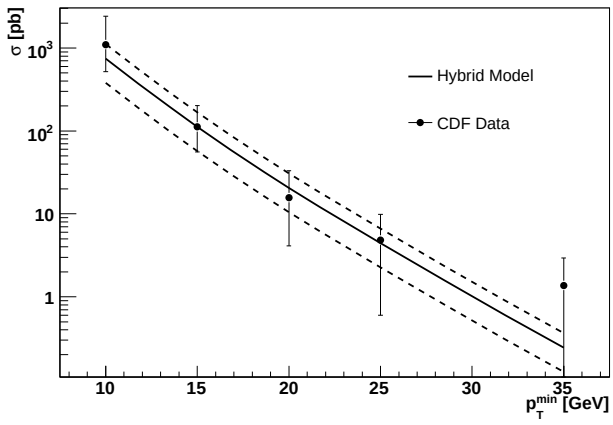


Fig. 5. Jet $E_{\mathrm{T\,min}}$ distribution for exclusive events measured by the CDF Collaboration compared with the hybrid model. The shape of the distribution is well reproduced by the model and the normalisation is fitted to the CDF measurement ($3.85 \times 10^{-4} \pm 1.89 \times 10^{-4}$).

for 5 data points and the uncertainty comes from the uncertainty on the CDF measurement. In Fig. 5, we give the prediction of HPM in full line, and the dashed line shows the uncertainty on normalisation ($\pm 1\sigma$) coming from the fit to the CDF data. We note that the shape of the HPM prediction describes nicely the CDF data while the normalisation comes directly from the CDF data as we mentioned previously.

In Fig. 6, we compare the predictions from the hybrid model to the dijet mass measurements in diffractive exclusive events from the CDF Collaboration. As explained in the CDF paper [4], this is an indirect measurement which is MC dependent due to the method used by the CDF Collaboration to extract the dijet mass cross-section. We follow the same method used by the CDF Collaboration to compute the dijet mass cross-section. Namely, we convert the measured exclusive dijet cross-section from CDF presented in Fig. 5 to a cross-section *versus* dijet mass using the HPM. After each $E_{\mathrm{T\,min}}$ cut (10, 15, 20, 25, and 35 GeV), we normalise the HPM cross-section to the CDF measurement. We have thus a "calibration" factor in each $E_{\mathrm{T\,min}}$ interval. The M_{JJ} distribution coming from the hybrid model is then reweighted after applying the $E_{\mathrm{T\,min}}$ cut using the same calibration factors. Removing the cuts on $E_{\mathrm{T\,min}}$ allows to obtain the "CDF points" given in Fig. 6. We followed basically the same procedure as in Ref. [4], but using the reweighted HPM instead of KMR. It is worth noticing that it is not strictly speaking a measurement by the CDF Collaboration since it is model dependent. Nevertheless, we can now compare the "CDF measurement" to the expectation of the hybrid model and the result is shown in Fig. 6. The dashed line indicates the uncertainties on the model related to the normalisation. The model leads to a good description of CDF data over the full dijet mass range.

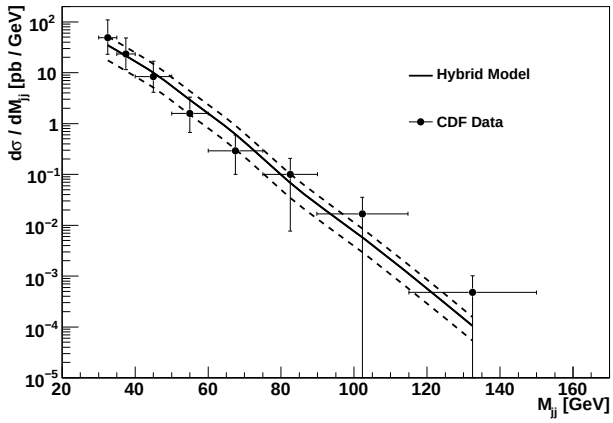


Fig. 6. Dijet mass distribution for exclusive events using the CDF method compared to the hybrid model. The normalisation comes from the fit to the CDF $E_{\mathrm{T\,min}}$ distribution (see Fig. 5) and the shape is well described by the hybrid model.

3.3. Uncertainties on the model predictions

In this section, we discuss the uncertainties related to the chosen values of parameters given in Table I. The first uncertainties come from the uncertainties on the parameter used to describe the hard interaction. As we mentioned already, the values of the parameters are taken from a fit to F_2 data coming from the HERA experiments [22]. The values of the parameters found in Ref. [22] where obtained with a given uncertainty coming from the fit procedure and it is worth checking the effect on the HPM predictions. There was also another kind of fits performed in Ref. [22] where heavy quarks were considered and we also compare our predictions including or not the heavy quarks. The values of the parameters are given in Table I for references. It is worth noticing that we use the same values of parameters coming from a fit to HERA data to extrapolate at LHC energies, especially when we predict the exclusive Higgs boson cross-section. It will be thus important to test the values of the parameters using directly LHC data when they will be available, and to study whether this assumption is valid. The effect of changing the hard parameters are given in Fig. 7 for the jet $E_{\mathrm{T\,min}}$ and the M_{JJ} distributions. The differences are found to be less than 20%.

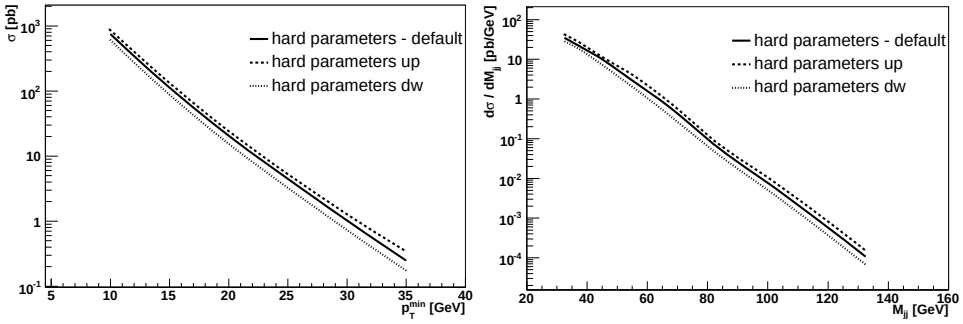


Fig. 7. Effect on modifying the hybrid model hard parameters on the $E_{\mathrm{T\,min}}$ and M_{JJ} cross-section distributions.

Another systematic study we performed was to change the b slope of the soft cross-section responsible for the soft interaction. The uncertainty on the b slope coming from soft data is quite small but we wanted to study the dependence of our model on this parameter. Modifying the b parameter from 2 to 4 leads to the cross-sections given in Fig. 8 for the jet $E_{\mathrm{T\,min}}$ and the M_{JJ} distributions. The difference is found to be less than 20% everywhere. It is worth noticing that the leading uncertainty in the predictions for HPM comes from the statistical uncertainties of the $E_{\mathrm{T\,min}}$ cross-section measurement by the CDF Collaboration which is of the order of 50%.

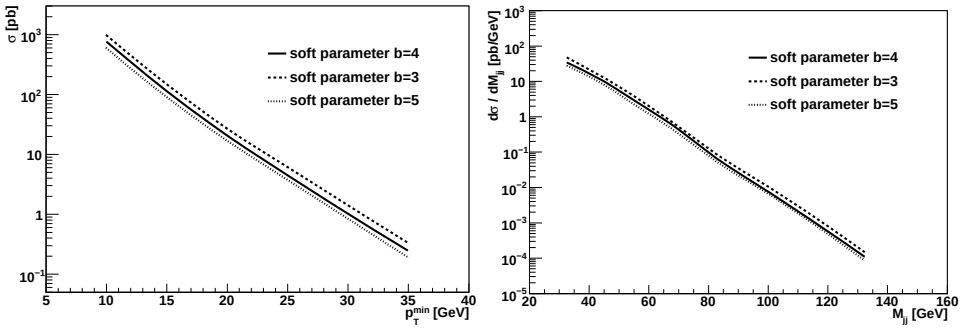


Fig. 8. Effect on modifying the hybrid model soft b parameters on the $E_{\mathrm{T}\,\mathrm{min}}$ and M_{JJ} cross-section distributions.

The effect of taking the parameters of the fit of Ref. [22] where heavy quarks are considered are given in Fig. 9. We recomputed the normalisation by fitting the $E_{\mathrm{T}\,\mathrm{min}}$ distribution to the CDF data and the normalisation for the light quark only model is $6.80 \times 10^{-3} \pm 3.46 \times 10^{-3}$ with a χ^2 of 0.83 for 5 data points. We notice that the mass dependence is stronger when heavy quarks are considered, which means that the cross-section at high mass is slightly smaller, and that the fit to the CDF data on $E_{\mathrm{T}\,\mathrm{min}}$ is slightly worse.

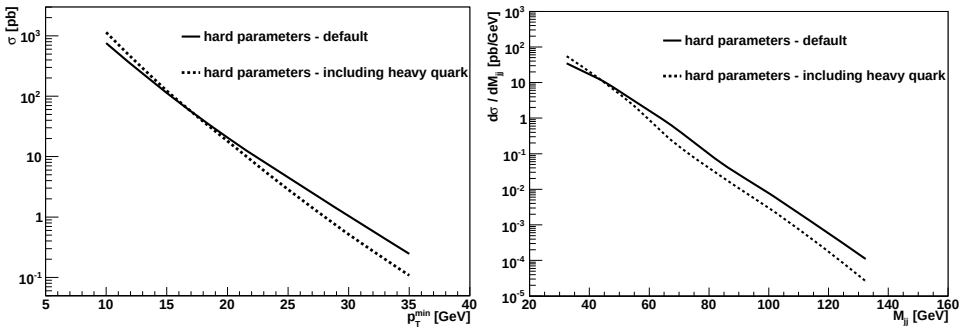


Fig. 9. Comparison of the jet $E_{\mathrm{T}\,\mathrm{min}}$ and M_{JJ} distributions for exclusive events with the hybrid model including or not heavy quark effects. The normalisation comes from a fit to the CDF exclusive $P_{\mathrm{T}\,\mathrm{min}}$ cross-section measurements. We note that including heavy quarks leads to a stronger $P_{\mathrm{T}\,\mathrm{min}}$ dependence.

3.4. Predictions for the LHC

In Fig. 10, we show the exclusive Higgs boson cross-section using the HPM. The cross-section varies from 1.1 ± 0.5 fb at 120 GeV to 0.32 ± 0.15 fb at 160 GeV. Including heavy quark effects reduces this cross-section by

about 60%. The values are found to be slightly lower than with the KMR model but compatible within uncertainties, and we should also notice that these predictions are at LO and it is known that NLL corrections increase the cross-section of typically about 20%.

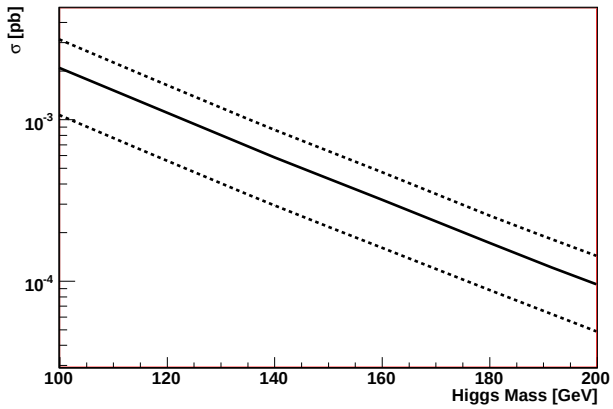


Fig. 10. Prediction on the diffractive exclusive Higgs cross-section at the LHC using the HPM.

In Fig. 11, we also compare the ξ distributions for jet production in exclusive events for the HPM and KMR models for jets with p_{T} >50 at the LHC. The ξ-slope is found to be smoother at the LHC for the KMR model than for the HPM. LHC data should thus allow to distinguish between both models or to tune better the parameters of the HPM given in the previous section.

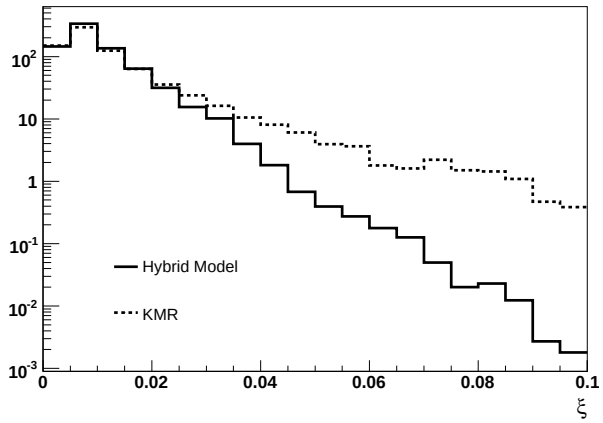


Fig. 11. ξ distribution for exclusive events for jets with $p_{\mathrm{T}} > 50$ GeV at the LHC for the KMR and HPM models. The ξ-dependence is smoother for KMR than for the HPM model. LHC data will help to distinguish and tune both models.

4. Conclusion

In this paper, we propose a new model to describe exclusive event production at hadronic colliders. It is based on Double Pomeron Exchange. We call it Hybrid Pomeron Model (HPM) since one of the color exchanges is considered to be hard, taking away most of the transverse momentum available while the colorless aspect of the overall crossed channel is ensured via a soft additional color exchange. The parameters of the model come from a fit to HERA F_2 data using a BFKL-based model for the hard part (eventually including saturation corrections), while the parameters of the soft part come from the usual soft cross-section models. The model was successfully implemented in a generator (FPMC) to be able to compare directly with the CDF measurements performed at particle level.

Our predictions are found to be in very good agreement with the measurements of the exclusive cross-section as a function of the minimum jet transverse momentum or the dijet mass from the CDF Collaboration. The HPM predicts a Higgs boson production cross-section of about 1.1 fb at the LHC for a Higgs boson mass of 120 GeV. This is in the same range and compatible with the KMR determination. The ξ distribution for exclusive events is softer for KMR than for the HPM model and it will be worth measuring it at the LHC and the Tevatron to distinguish and further tune both models. As we mentioned, the parameters used in the HPM come from an extrapolation from a fit to HERA data and it will be good to cross check the values of the parameters using direct data from the LHC.

We thank Cyrille Marquet for useful remarks. One of us (M.R.) acknowledges support from CNPq (Brazil).

REFERENCES

[1] C. Royon [RP220 Collaboration], `arXiv:0706.1796 [physics.ins-det]`; M.G. Albrow *et al.* [FP420 R&D Collaboration], `arXiv:0806.0302 [hep-ex]`.

[2] M G. Albrow, A. Rostovtsev, `arXiv:hep-ph/0009336`.

[3] V.A. Khoze, A.D. Martin, M.G. Ryskin, *Eur. Phys. J* **C55**, 363 (2008); *Phys. Lett.* **B650**, 41 (2007).

[4] CDF Collaboration, *Phys. Rev.* **D77**, 052004 (2008).

[5] O. Kepka, C. Royon, *Phys. Rev.* **D76**, 034012 (2007).

[6] J.D. Bjorken, *Phys. Rev.* **D47**, 101 (1993); J.R. Cudell, O.F. Hernandez, *Nucl. Phys.* **B471**, 471 (1996); E.M. Levin, `hep-ph/9912403` and references therein; J. Pumplin, *Phys. Rev.* **D52**, 1477 (1995); A. Berera, J.C. Collins, *Nucl. Phys.* **474**, 183 (1996).

[7] R. Enberg, G. Ingelman, A. Kissavos, N. Timneanu, *Phys. Rev. Lett.* **89**, 081801 (2002).

[8] A. Bialas, P.V. Landshoff, *Phys. Lett.* **B 256**, 540 (1991).

[9] M. Boonekamp, R. Peschanski, C. Royon, *Phys. Rev. Lett.* **87**, 251806 (2001); M. Boonekamp, A. De Roeck, R. Peschanski, C. Royon, *Phys. Lett.* **B550**, 93 (2002); M. Boonekamp, R. Peschanski, C. Royon, *Nucl. Phys.* **B669**, 277 (2003); Erratum, *Nucl. Phys.* **B676**, 493 (2004); for a general review see C. Royon, *Mod. Phys. Lett.* **A18**, 2169 (2003).

[10] M. Boonekamp, R. Peschanski, C. Royon, *Phys. Lett.* **B598**, 243 (2004).

[11] V.A. Khoze, A.D. Martin, M.G. Ryskin, *Eur. Phys. J.* **C19**, 477 (2001); Erratum, *Eur. Phys. J.* **C20**, 599 (2001); V.A. Khoze, A.D. Martin, M.G. Ryskin, *Eur. Phys. J.* **C24** (2002) 581.

[12] J.R. Forshaw, Diffractive Higgs Production: Theory, `arXiv:hep-ph/0508274`.

[13] V.A. Khoze, A.D. Martin, M.G. Ryskin, W.J. Stirling, *Eur. Phys. J.* **C35**, 211 (2004); M. Rangel, C. Royon, G. Alves, J. Barreto, R. Peschanski, *Nucl. Phys.* **B774**, 53 (2007).

[14] V.S. Fadin, E.A. Kuraev, L.N. Lipatov, *Phys. Lett.* **B60**, 50 (1975); E.A. Kuraev, L.N. Lipatov, V.S. Fadin, *Sov. Phys. JETP* **45**, 199 (1977) [*Zh. Eksp. Teor. Fiz.* **72**, 377 (1977)]; I.I. Balitsky, L.N. Lipatov, *Sov. J. Nucl. Phys.* **28**, 822 (1978) [*Yad. Fiz.* **28**, 1597 (1978)]; L.N. Lipatov, *Sov. Phys. JETP* **63**, 904 (1986) [*Zh. Eksp. Teor. Fiz.* **90**, 1536 (1986)]; V.S. Fadin, L.N. Lipatov, *Phys. Lett.* **B429**, 127 (1998); M. Ciafaloni, *Phys. Lett.* **B429**, 363 (1998); M. Ciafaloni, G. Camici, *Phys. Lett.* **B430**, 349 (1998).

[15] A. Bialas, R.B. Peschanski, C. Royon, *Phys. Rev.* **D57**, 6899 (1998); H. Navelet, R. Peschanski, C. Royon, S. Wallon, *Phys. Lett.* **B385** (1996) 357.

[16] C. Marquet, *Phys. Rev.* **D76**, 094017 (2007).

[17] P.V. Landshoff, O. Nachtmann, *Z. Phys.* **C35**, 405 (1987).

[18] C. Marquet, R.B. Peschanski, G. Soyez, *Phys. Rev.* **D76**, 034011 (2007).

[19] A. Kupco, C. Royon, R. Peschanski, *Phys. Lett.* **D606**, 139 (2005).

[20] J.D. Bjorken, *Phys. Rev.* **D47**, 101 (1993); E. Gotsman, E. Levin, U. Maor, *Phys. Lett.* **B438**, 229 (1998); A.B. Kaidalov, V.A. Khoze, A.D. Martin, M.G. Ryskin, *Eur. Phys. J.* **C21**, 521 (2001); A. Bialas, *Acta Phys. Pol. B* **33**, 2635 (2002); A. Bialas, R. Peschanski, *Phys. Lett.* **B575**, 30 (2003).

[21] A. Donnachie, P.V. Landshoff, *Phys. Lett.* **B207**, 319 (1988).

[22] G. Soyez, *Phys. Lett.* **B655**, 32 (2007).

[23] S. Munier, R.B. Peschanski, *Phys. Rev. Lett.* **91**, 232001 (2003); *Phys. Rev.* **D69**, 034008 (2004); *Phys. Rev.* **D70**, 077503 (2004).

[24] E. Iancu, K. Itakura, S. Munier, *Phys. Lett.* **B590**, 199 (2004).

[25] J. Forshaw, Proceedings of Ringberg, 2008.

[26] C. Adloff *et al.* [H1 Collaboration], *Eur. Phys. J.* **C21**, 33 (2001); J. Breitweg *et al.* [ZEUS Collaboration], *Phys. Lett.* **B487**, 273 (2000); S. Chekanov *et al.* [ZEUS Collaboration], *Eur. Phys. J.* **C21**, 443 (2001); C. Adloff *et al.* [H1 Collaboration], *Phys. Lett.* **B528**, 199 (2002); A. Aktas *et al.* [H1 Collaboration], *Eur. Phys. J.* **C45**, 23 (2006); S. Chekanov *et al.* [ZEUS Collaboration], *Phys. Rev.* **D69**, 012004 (2004).

[27] A. Bialas, W. Szeremeta, *Phys. Lett.* **B296**, 191 (1992); W. Szeremeta, *Acta Phys. Pol. B* **24**, 1159 (1993).

[28] M. Boonekamp, V. Juranek, O. Kepka, M. Rangel, C. Royon, in preparation; see `http://cern.ch/project-fpmc/`

[29] G. Marchesini *et al.*, *Comput. Phys. Commun.* **67**, 465 (1992).

[30] G.C. Blazey *et al.*, Run II Jet Physics, `arXiv:hep-ex/0005012`.